Nonlinear Modelling and Robust Backstepping Control of a Quadcopter in Aggressive Maneuvering

Mehmet KARAHAN
TOBB University of Economics and Technology, 43 Sogutozu Avenue, Ankara, 06510, Turkey
mehmetkarahan@etu.edu.tr

Abstract: Quadcopter unmanned aerial vehicles (UAVs) are vehicles with 4 propellers, capable of taking off and landing vertically (VTOL) and hovering in the air. In recent years, developments in hardware, software, battery, sensor and camera technologies have facilitated the production processes of quadcopters and led to diversified usage areas. Quadcopters are used in many different areas such as fighting natural disasters, combating terrorism, border patrol, surveillance, search and rescue and cargo transportation. Quadcopters need to be fast and able to make aggressive maneuvers, when performing these tasks. In this study, nonlinear modelling of the quadcopter was carried out and a robust backstepping controller was designed, which allows the quadcopter to make harsh maneuvers. The quadcopter has been tested under triangular, sinusoidal and sawtooth maneuvers. A 10% parameter uncertainty was also implemented to the mass (m) and inertial moments (Ix, Iy and Iz) of the quadcopter during aggressive maneuver tracking. The backstepping controller proposed in the study was compared with classical PID and Lyapunov-based control methods. A comprehensive robustness examination was realized by obtaining time response of all controllers, while performing harsh maneuvers. Thus, the superiority of backstepping control under aggressive maneuvers has been shown.

Keywords: Quadcopter, PID control, Lyapunov-based control, Backstepping control, Robust control, Aggressive maneuver.

1. Introduction

Quadcopter UAVs are widely used in many different areas today. Agricultural spraying, reconnaissance, anti-terrorism, firefighting, mining, first aid, transportation and aerial photography are some important areas where they are used (Sonugur, 2023; Karahan et al., 2023).

Quadcopter UAVs' ability to VTOL, to remain hovered in the air, to rotate around their own axis, and to take off and land without the need for a runway make them more advantageous than other UAVs (Saeed et al., 2018; Frigioescu et al., 2023).

Quadcopter UAVs must be fast and able to perform aggressive maneuvers, while performing different missions. For this reason, it becomes important to design a robust controller that can control the altitude and attitude of the quadcopter, while performing harsh maneuvers.

Many researchers have designed robust controllers to enable quadcopters to follow different trajectories. Kidambi et al. (2021) used a Lyapunov-based controller to track different references under uncertainties, while they neglected drag and aerodynamic effects. Mehmood et al. (2021) used a super twisting sliding mode controller design for multiple quadcopter UAVs and tracked sinusoidal and circular references under parameter uncertainties and disturbances. AbdulSamed et al. (2020) used a PID controller to track different references for a quadcopter UAV. In some of their simulations, the quadcopter followed the unit step reference, and, in other simulations, it reached the target by passing through some points. Additionally, they neglected aerodynamic effects in their studies.

Pan et al. (2023) proposed an adaptive sliding mode controller for the attitude control of a quadcopter and compared the results of the simulations with those of the experimental platform. Elhesasy et al. (2023) developed a model predictive controller (MPC) for a quadcopter and tested it under model uncertainties and disturbances. They observed that MPC controller showed better performance than PID controller. Liu et al. (2023) focused on developing a fuzzy attitude control structure for a quadcopter. They realized comparative simulations and experiments. Nekoo et al. (2022) developed a sliding mode control for a quadcopter and compared the performance of this controller with that of the PD controller. They performed the cobra maneuver by rotating the quadcopter vertically at an angle of $\theta=\pi/2$. In their simulations, they observed that the sliding mode control performed better.

Sun et al. (2021) developed a cascaded PID controller to control a quadcopter. They performed a simulation that required a smooth maneuver, following the 3rd order Bezier curve, and a simulation that required a hard maneuver, following the 3rd order polynomial. Wang et al. (2022) proposed an adaptive sliding mode controller for a smooth geometric trajectory tracking of a quadcopter UAV. Zhao et al. (2020) developed a sliding mode control for a quadcopter

https://doi.org/10.24846/v33i3y202403

and tested it through numerical simulations. They tested the controller in following a helix trajectory and determined the error rate of the quadcopter, while following the trajectory.

In this research, firstly, modelling of the quadcopter was carried out. The drag coefficient or aerodynamic effects were not neglected, and no linearization was made. Then, PID, Lyapunov-based and backstepping controller designs were realized, respectively. Aggressive maneuver tracking simulations were carried out by giving triangular, sinusoidal and sawtooth references to the system. During aggressive maneuver tracking, 10% parameter uncertainty was also applied to m, I_x, I_y *and* I_z values. A comparative robustness analysis was performed, by obtaining time response of controllers. Thus, the superiority of the backstepping control has been numerically demonstrated.

The present study is structured as follows. Section 2 presents the nonlinear quadcopter model. The control structures are described in section 3. Then, section 4 treats the simulations and their results, and, finally, section 5 offers the conclusion of this study.

2. Nonlinear Quadcopter Model

Quadcopter is a UAV which could move in 6 degrees of freedom. While translational movements are indicated by movements in the x, y, z axes, rotational movements are indicated by roll, pitch, yaw. The (1,3) and (2,4) propeller pairs of the quadcopter rotate oppositely. A schematic presentation of the quadcopter used in this study is shown in Figure 1.

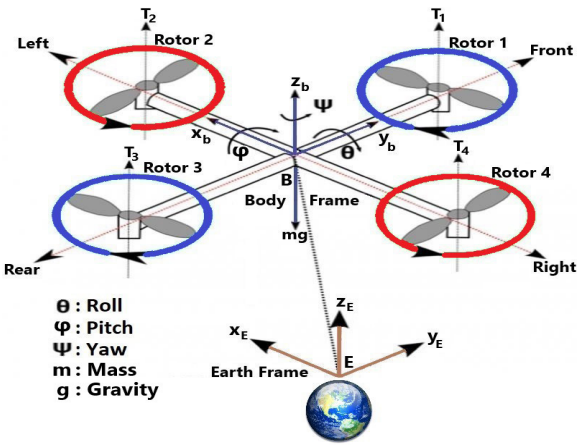

Figure 1. Schematic of the quadcopter (Karahan & Kasnakoglu, 2021)

Rotation matrix transforms the body frame axis into the Earth frame axis. The extraction of the rotation matrix used in this transformation is shown step by step in equations (1) – (5). In the equations, s represents the sine angle and c represents the cosine angle.

$$R(\varphi)=\begin{bmatrix}1 & 0 & 0\\ 0 & c(\varphi) & s(\varphi)\\ 0 & -s(\varphi) & c(\varphi)\end{bmatrix} \tag{1}$$

$$R(\theta)=\begin{bmatrix}c(\theta) & 0 & -s(\theta)\\ 0 & 1 & 0\\ s(\theta) & 0 & c(\theta)\end{bmatrix} \tag{2}$$

$$R(\psi)=\begin{bmatrix}c(\psi) & s(\psi) & 0\\ -s(\psi) & c(\psi) & 0\\ 0 & 0 & 1\end{bmatrix} \tag{3}$$

$$R(\varphi,\theta,\psi)=R(\varphi)R(\theta)R(\psi) \tag{4}$$

$$R=\begin{bmatrix}c\psi c\theta & s\psi c\theta & -s\theta\\ c\psi s\theta s\varphi - s\psi c\varphi & s\psi s\theta s\varphi + c\psi c\varphi & c\theta s\varphi\\ c\psi s\theta c\varphi + s\psi s\varphi & s\psi s\theta c\varphi - c\psi s\varphi & c\theta c\varphi\end{bmatrix} \tag{5}$$

Conversion from body angular rates to Earth angle rates is represented in equations (6) and (7), where T is the transformation matrix, p, q, r symbolize the angular rates in the body frame and $\dot{\varphi}$, $\dot{\theta}$, and $\dot{\psi}$ represent the angular rates in Earth frame.

$$T=\begin{bmatrix}1 & \tan(\theta)s(\varphi) & \tan(\theta)c(\varphi)\\ 0 & c(\varphi) & -s(\varphi)\\ 0 & \sec(\theta)s(\varphi) & \sec(\theta)c(\varphi)\end{bmatrix} \tag{6}$$

$$\begin{bmatrix}\dot{\varphi}\\ \dot{\theta}\\ \dot{\psi}\end{bmatrix}=T\begin{bmatrix}p\\ q\\ r\end{bmatrix} \tag{7}$$

In (7), $\theta \neq \frac{\pi}{2}$ because of derivatives. When φ and θ angles are near to zero, this indicates that quadcopter is hovering, and T becomes the unit matrix. In this case, the connection with angles and angular rates could be taken linear as in equation (8):

$$\begin{bmatrix}\dot{\varphi}\\ \dot{\theta}\\ \dot{\psi}\end{bmatrix}\approx\begin{bmatrix}p\\ q\\ r\end{bmatrix} \tag{8}$$

Equation (9) explains torque, equation (10) represents force and equation (11) gives relative rotor speed. In below equations, *i* subscript indicates rotor number (1, 2, 3, 4), *b* represents thrust coefficient and *d* symbolizes drag coefficients.

$$F_i = bw_i^2 \tag{9}$$

$$T_i = dw_i^2 \tag{10}$$

$$w_r = -w_1 + w_2 - w_3 + w_4 \tag{11}$$

Equation (12) shows conversion from system inputs to angular rates. U_1, U_2, U_3, U_4 present control inputs and l gives arm length of the quadcopter. U_1 explains lift force and U_2, U_3, U_4 indicate relevant torque values.

$$u = \begin{bmatrix} U_1 \\ U_2 \\ U_3 \\ U_4 \end{bmatrix} = \begin{bmatrix} F \\ T_\varphi \\ T_\theta \\ T_\psi \end{bmatrix} = \begin{bmatrix} b & b & b & b \\ 0 & -lb & 0 & lb \\ lb & 0 & -lb & 0 \\ -d & d & -d & d \end{bmatrix} \begin{bmatrix} w_1^2 \\ w_2^2 \\ w_3^2 \\ w_4^2 \end{bmatrix} \tag{12}$$

Equation (13) shows the conversion between angular rates and control inputs.

$$\begin{bmatrix} w_1^2 \\ w_2^2 \\ w_3^2 \\ w_4^2 \end{bmatrix} = \begin{bmatrix} 1/4b & 0 & 1/2bl & -1/4d \\ 1/4b & -1/2bl & 0 & 1/4d \\ 1/4b & 0 & -1/2bl & -1/4d \\ 1/4b & 1/2bl & 0 & 1/4d \end{bmatrix} \begin{bmatrix} U_1 \\ U_2 \\ U_3 \\ U_4 \end{bmatrix} \tag{13}$$

The inertial moments of the quadcopter are shown in equations (14) – (16), where *Msphere* is the spherical dense center mass, *r* is the radius and *Mrotor* symbolizes the rotor mass (Krishna et al., 2022).

$$I_x = \frac{2}{5} M_{sphere} r^2 + 2l^2 M_{rotor} \tag{14}$$

$$I_y = \frac{2}{5} M_{sphere} r^2 + 2l^2 M_{rotor} \tag{15}$$

$$I_z = \frac{2}{5} M_{sphere} r^2 + 4l^2 M_{rotor} \tag{16}$$

Figure 2 represents the spherical mass and rotor masses of quadcopter.

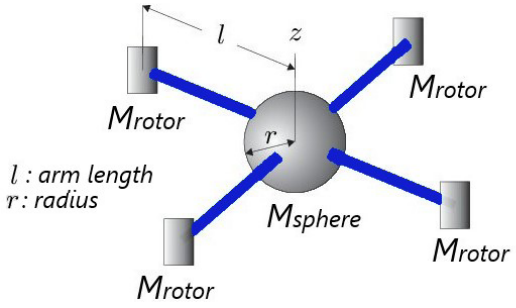

Figure 2. Presentation of quadcopter masses (Karahan & Kasnakoglu, 2021)

The equations showing the movements of the quadcopter in 6 degrees of freedom are shown in equations (17) – (22).

$$\ddot{X} = \frac{U_1}{m}[c(\varphi)s(\theta)c(\psi) + s(\varphi)s(\psi)] \tag{17}$$

$$\ddot{Y} = \frac{U_1}{m}[s(\theta)s(\psi)c(\varphi) - s(\varphi)c(\psi)] \tag{18}$$

$$\ddot{Z} = -g + \frac{U_1}{m}[c(\varphi)c(\theta)] \tag{19}$$

$$\ddot{\varphi} = \frac{1}{I_x} U_2 + \left(\frac{I_y - I_z}{I_x}\right)\dot{\psi}\dot{\theta} + w_r \frac{J_R}{I_x}\dot{\theta} \tag{20}$$

$$\ddot{\theta} = \frac{1}{I_y} U_3 + \left(\frac{I_z - I_x}{I_y}\right)\dot{\theta}\dot{\psi} + w_r \frac{J_R}{I_y}\dot{\varphi} \tag{21}$$

$$\ddot{\psi} = \frac{1}{I_z} U_4 + \left(\frac{I_x - I_y}{I_z}\right)\dot{\theta}\dot{\varphi} \tag{22}$$

Physical specifications of the OS4 quadcopter employed in the study are given in Table 1.

Table 1. Quadcopter Specifications

Unit	Value
Quadcopter mass (m)	0.65 kg
Gravitational acceleration (g)	9.81 m/s^2
Arm length (l)	0.23 m
Maximum rotor velocity (w_{max})	1000 rad/sec
Maximum torque (t_{max})	0.15 Nm
Thrust coefficient (b)	3.13x10^{-5} Ns^2
Drag coefficient (d)	7.5x10^{-7} Ns^2
Rotor moment of inertia (J_R)	6.5x10^{-5} kg.m^2
Moment of inertia on x axis (I_x)	7.5x10^{-3} kg.m^2
Moment of inertia on y axis (I_y)	7.5x10^{-3} kg.m^2
Moment of inertia on z axis (I_z)	1.3x10^{-2} kg.m^2

3. Control Structures

The classical PID control approach, Lyapunov-based control approach and backstepping control method, respectively, are presented in the following subsections.

3.1 Classical PID Control Approach

PID control method is explained in this part. It has three coefficients, namely K_p, K_i and K_d (Dobrea et al., 2023). The PID controller block was created in Simulink. K_p, K_i and K_d coefficients were determined by manually adjusting the PID Tuner feature in Simulink. While determining the coefficients, it was aimed to obtain low overshoot and a short settling time. Since the PID Tuner interface displays the system response graphically, it makes it easier to understand the effect of the change in controller coefficients on the system response. In this way, optimum coefficients were

determined by using the graphical interface. This control approach efforts to reduce error term *e(t)* by utilizing *u(t)* control term. The overall function of this controller is given in equation (23):

$$u(t) = K_p e(t) + K_i \int_0^t e(\tau)d\tau + K_d \frac{de(t)}{dt} \quad (23)$$

PID control inputs are given in equations (24) – (27). U_1 control input controls the altitude. U_2, U_3 and U_4 control inputs control roll angle, pitch angle and yaw angle, respectively.

$$U_1 = \frac{m(g + e_z K_p + K_i \int e_z dt + K_d \frac{de_z}{dt})}{\cos\varphi \cos\theta} \quad (24)$$

$$U_2 = e_\varphi K_p + K_i \int e_\varphi dt + K_d \frac{de_\varphi}{dt} \quad (25)$$

$$U_3 = e_\theta K_p + K_i \int e_\theta dt + K_d \frac{de_\theta}{dt} \quad (26)$$

$$U_4 = e_\psi K_p + K_i \int e_\psi dt + K_d \frac{de_\psi}{dt} \quad (27)$$

In equation (24), θ and φ angles indicate rotation around y and x axes, respectively. Because the quadcopter could not rotate around the x and y axes while flight vertically, denominator of equation (24) will never be zero. PID control parameters are presented in Table 2.

Table 2. PID parameters

Parameter	Roll	Pitch	Yaw	Altitude
K_p	0.11	0.13	0.03	0.83
K_i	0.04	0.06	0.02	0.10
K_d	0.05	0.07	0.06	1.66

3.2 Lyapunov-based Control Approach

Lyapunov-based control depends on Lyapunov stability theorem (Lavaei & Bridgeman, 2023). It uses a Lyapunov function to directly control a nonlinear system. In this study, the Lyapunov-based control method targets direct control of the quadcopter's position. In this method, x = 0 is selected as the equilibrium point. *D* is described as a strict neighborhood of *f(0)* in R^n. The continuous Lyapunov function $V: D \rightarrow R^+$, which meets the necessities expressed in equations (28) and (29), is determined.

$$V(0) = 0,\ V(x) > 0 \ in\ D, x \neq 0 \quad (28)$$

$$\dot{V}(x) \leq 0 \ in\ D \quad (29)$$

Equilibrium point becomes asymptotically steady in *D* under given $\dot{V}(x) \leq 0$ *in D,* $x \neq 0$ conditions. Then, a section which includes stabilization angles and derivates, is described as desired attitude at the equilibrium point. At this point, x = (φ_d, 0, θ_d, 0, ψ_d, 0), where φ_d, θ_d and ψ_d angles are described as the desired roll, pitch and yaw angles, respectively. Because the angular velocity components are 0 at the stabilization point, their time derivatives are also 0. Positive defined Lyapunov function at desired attitude is presented in (30):

$$V(x) = \frac{1}{2}[\dot{\varphi}^2 + (\varphi - \varphi_d)^2 + \dot{\theta}^2 + (\theta - \theta_d)^2 + \dot{\psi}^2 + (\psi - \psi_d)^2] \quad (30)$$

Derivative of *V(x)* is shown in (31):

$$\dot{V}(x) = [(\varphi - \varphi_d)\dot{\varphi} + \ddot{\varphi}\dot{\varphi} + (\theta - \theta_d)\dot{\theta} + \ddot{\theta}\dot{\theta} + (\psi - \psi_d)\dot{\psi} + \ddot{\psi}\dot{\psi}] \quad (31)$$

Equations of motions given in (17 – 22) can be reduced under perfect cross condition (I_x=I_y), when the quadcopter is near to the equilibrium point (w_r = 0, $\dot{\psi}$ = 0, $\dot{\theta}$ = 0, $\dot{\varphi}$ = 0) and equation (32) is acquired:

$$\dot{V}(x) = (\varphi - \varphi_d)\dot{\varphi} + \dot{\varphi}\frac{l}{I_x}U_2 + (\theta - \theta_d)\dot{\theta} + \dot{\theta}\frac{l}{I_y}U_3 + (\psi - \psi_d)\dot{\psi} + \dot{\psi}\frac{l}{I_z}U_4 \quad (32)$$

The control inputs for the stability criteria are described by the following equations:

$$U_2 = -\frac{I_x}{l}(\varphi - \varphi_d) - k_1\dot{\varphi} \quad (33)$$

$$U_3 = -\frac{I_y}{l}(\theta - \theta_d) - k_2\dot{\theta} \quad (34)$$

$$U_4 = -I_z(\psi - \psi_d) - k_3\dot{\psi} \quad (35)$$

By substituting the above inputs in (32), this equation could be revised as below:

$$\dot{V}(x) = -\dot{\varphi}^2\frac{l}{I_x}k_1 - \dot{\theta}^2\frac{l}{I_y}k_2 - \dot{\psi}^2\frac{l}{I_z}k_3 \quad (36)$$

where k_1, k_2 and k_3 are the positive constants described in equations (33) – (36) that are negative semidefinite. The stability for equilibrium point is guaranteed as a result of the Lyapunov theory. Stability is ensured by employing the invariance criteria, since the controlled maximum invariant set of subsystems in $S = \{X \in R^6 : \dot{V} \mid x = 0\}$ is limited by the equilibrium point (Zhou et al., 2023). For altitude control, Lyapunov function and its derivative are given in (37) and (38):

$$V(x) = \frac{1}{2}[(z - z_d)^2 + \dot{z}^2] \quad (37)$$

$$\dot{V}(x) = (z - z_d)\dot{z} + \dot{z}(g - (\cos\theta\cos\varphi)\frac{U_1}{m}) \quad (38)$$

U_1 control input is described in (39) for stability criteria.

$$U_1 = -\frac{m}{\cos\theta\cos\varphi}(z_d - z - g) - k_z\dot{z} \quad (39)$$

When U_1 is substituted in (38), (40) is acquired. k_z is a positive constant presented by (39) which is negative semidefinite.

$$\dot{V}(x) = -\dot{z}^2\frac{k_z}{m}(\cos\theta\cos\varphi) \quad (40)$$

Coefficients of Lyapunov-based control are presented in Table 3. k_1, k_2 and k_3 are parameters of the roll, pitch, yaw controllers, respectively. k_z represents the parameter of the altitude control. The Lyapunov-based controller was modeled using the Simulink program. Lyapunov controller parameters were determined manually by trial and error. While determining the controller coefficients, it was aimed to obtain the least overshoot and the fastest settling time.

Table 3. Parameters of the Lyapunov-based control

Parameter	Value
k_1	0.167
k_2	0.168
k_3	0.104
k_z	2.15

3.3 Backstepping Control Approach

Backstepping control method is an adaptive control approach (Zhang et al., 2021). It relies on a recursive method which connects the choosing of Lyapunov function with feedback control mechanism and allows strict-feedback for reaching stability. Lyapunov's direct method is used with basics of adaptive control. Firstly, z_1 error is described as in (41):

$$z_1 = \varphi_d - \varphi \quad (41)$$

Lyapunov equation and its derivative for z_1 are given in (42) and (43):

$$V(z_1) = \frac{1}{2}z_1^2 \quad (42)$$

$$\dot{V}(z_1) = z_1(\dot{\varphi}_d - \dot{\varphi}) \quad (43)$$

Because the derivative of Lyapunov equation should be negative semidefinite, a new virtual control input $\dot{\varphi}$ is defined to stabilize z_1 as in (44):

$$\dot{\varphi} = \dot{\varphi}_d + a_1 z_1 \quad (44)$$

a_1 coefficient should be positive to obtain negative semidefiniteness. When the virtual control term is put in (43), equation (45) is obtained.

$$\dot{V}(z_1) = -a_1 z_1^2 \quad (45)$$

Another variable change is given in equation (46):

$$z_2 = \dot{\varphi} - \dot{\phi}_d - a_1 z_1 \quad (46)$$

Afterwards the replacements, augmented Lyapunov equation can be given in (47):

$$V(z_1, z_2) = \frac{1}{2}z_1^2 + \frac{1}{2}z_2^2 \quad (47)$$

Lyapunov equation's derivative could be described in (48):

$$\dot{V}(z_1, z_2) = -a_1 z_1^2 - z_1 z_2 + z_2\ddot{\varphi} - z_2(\ddot{\varphi}_d - a_1(z_2 + a_1 z_1)) \quad (48)$$

In accordance with equation (20), $\ddot{\varphi}$ variable could be written as in equation (49):

$$\ddot{\varphi} = \psi\dot{\theta}a_1 + a_2\dot{\theta}w_r + \frac{l}{I_x}U_2 \quad (49)$$

U_2 input is described as (50) under $\ddot{\varphi} = 0$, $\ddot{\varphi} = 0$, $\ddot{\theta}_d = 0$ and $\dot{V}(z_1, z_2) < 0$ conditions.

$$U_2 = \frac{I_x}{l}(z_1 - a_1\dot{\theta}\dot{\psi} - a_2\dot{\theta}w_r - a_1(z_2 + a_1 z_1) - a_2 z_2) \quad (50)$$

The $a_2 z_2$ expression with $a_2 > 0$ is added to stabilize z_1. With the same methods, U_3 and U_4 inputs are described as in (51) and (52):

$$U_3 = \frac{I_y}{l}(z_3 - a_3\dot{\varphi}\dot{\psi} - a_4\dot{\varphi}w_r - a_3(z_4 + a_3 z_3) - a_4 z_4) \quad (51)$$

$$U_4 = I_z(z_5 - a_5\dot{\varphi}\dot{\theta} - a_5(z_6 + a_5 z_5) - a_6 z_6) \quad (52)$$

Equations (53) – (56) describe variables utilized in U_3 and U_4.

$$z_3 = \theta_d - \theta \quad (53)$$

$$z_4 = \dot{\theta} - \dot{\theta}_d - a_3 z_3 \quad (54)$$

$$z_5 = \psi_d - \psi \quad (55)$$

$$z_6 = \dot{\psi} - \dot{\psi}_d - a_5 z_5 \quad (56)$$

The tracking error of altitude control is shown as z_7.

$$z_7 = z - z_d \quad (57)$$

The Lyapunov function for z_7 and its derivative are given in (58) and (59):

$$V(z_7) = \frac{1}{2} z_7^2 \tag{58}$$

$$\dot{V}(z_7) = z_7(\dot{z}_d - \dot{z}) \tag{59}$$

The x_8 virtual control input, given in (60), is used to stabilize z_7 variable.

$$x_8 = \dot{z}_d + a_7 z_7 \tag{60}$$

Another variable change is presented in (61):

$$z_8 = x_8 - \dot{z}_d - a_7 z_7 \tag{61}$$

After the variable replacements are completed, new Lyapunov equation is defined in (62):

$$V(z_7, z_8) = \frac{1}{2} z_7^2 + \frac{1}{2} z_8^2 \tag{62}$$

The above Lyapunov equation's derivative can be given as in (63):

$$\dot{V}(z_7, z_8) = -a_7 z_7^2 - z_7 z_8 + z_8 x_8 - z_8(\ddot{z}_d - a_7(z_8 + a_7 z_7)) \tag{63}$$

The derivative of *x8* virtual control term is defined as in (64):

$$\dot{x}_8 = g - \cos\theta \cos\varphi \frac{U_1}{m} \tag{64}$$

The U_1 control term that controls altitude is presented in (65):

$$U_1 = \frac{m}{\cos\theta \cos\varphi}(z_7 + g - a_7(z_8 + a_7 z_7) - a_8 z_8) \tag{65}$$

Table 4 illustrates parameters of backstepping control. The backstepping controller is modeled using Simulink program. The coefficients of the controller were found by trial and error. While determining the coefficients, it was aimed to obtain the least overshoot and the shortest settling time.

Table 4. Parameters of backstepping control

Variable	Roll	Pitch	Yaw	Altitude
(a_1,…,a_8)	(8.68, 6.99)	(8.2, 3.95)	(8.45, 4.05)	(1.45, 5.95)

4. Simulations

Aggressive maneuver simulations were realized using the MATLAB program. The ability of controllers designed for quadcopter to follow sinusoidal, triangle and sawtooth references was examined. Time response data of PID, Lyapunov-based and backstepping controllers were found and compared. In the simulations, rise time was determined as the time required for the controller to reach from 10% to 90% of the final value of the given reference. Overshoot refers to an output exceeding its final, steady-state value in terms of percent. Settling time is taken as the time when the system response reaches the final value within the 5% tolerance band and settles. In the simulations, roll, pitch, and yaw references were determined in radians, height in meters, and time in seconds. Rise time, overshoot and settling time data of PID, Lyapunov-based and backstepping controllers were obtained and compared with each other for different reference types. Thus, a comparative analysis was realized and robustness of the developed backstepping controller was demonstrated numerically. Figure 3 displays the block diagram of quadcopter system created in Simulink.

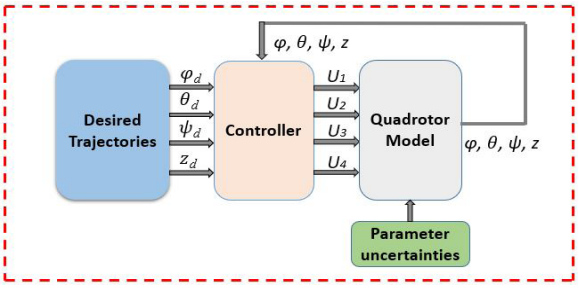

Figure 3. Block diagram of the employed system (Karahan et al., 2023)

4.1 Triangular Wave Simulations

In this subsection, reference tracking simulations were made using a triangular wave with amplitude 2 and period 2. Figures (4) to (7) show triangular reference tracking simulations of the controllers.

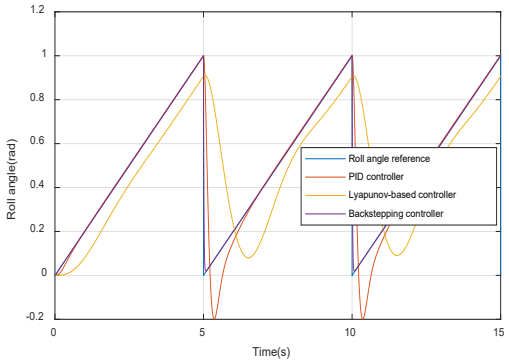

Figure 4. Roll tracking for triangular reference

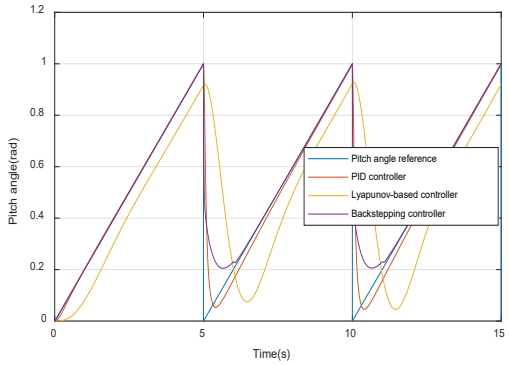

Figure 5. Pitch tracking for triangular reference

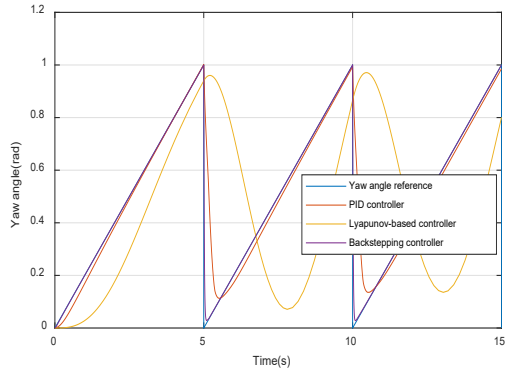

Figure 6. Yaw tracking for triangular reference

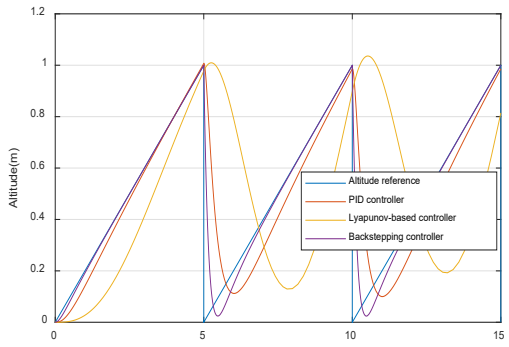

Figure 7. Altitude tracking for triangular reference

Table 5 contains the controllers' time response data for triangular reference tracking.

According to Table 5, the PID controller shows the highest overshoot value and the longest settling time value. The Lyapunov-based control shows the least rise time and does not show overshoot, except for the altitude reference. However, since the given references cannot settle within the ± 5% range, there is no settling time in any of the references. Since the backstepping controller follows the triangle reference almost without error from the beginning of the simulation, the settling time is 0 seconds, except for the pitch and altitude references. The backstepping control is the best control because it does not show overshoot and shows the fastest settling time.

4.2 Sinusoidal Wave Simulations

The following reference was performed under a sinusoidal wave of 3 rad/s. Sinusoidal reference tracking simulations are given in Figures (8) to (11).

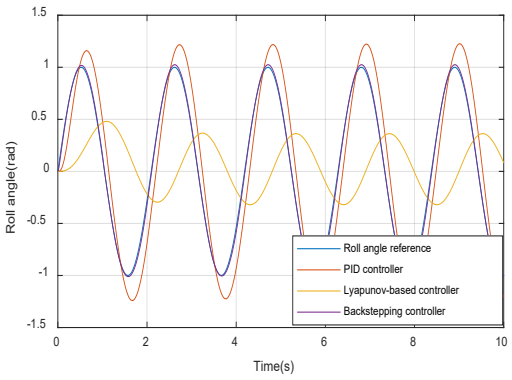

Figure 8. Roll tracking for sinusoidal reference

Table 5. Time response for triangular reference

Controller	Rise time (s)	Overshoot (%)	Settling time (s)
Roll PID	3.99	22	6.19
Roll Lyapunov-based	3.89	0	-
Roll Backstepping	3.98	0	0
Pitch PID	4.01	0	7.05
Pitch Lyapunov-based	3.85	0	-
Pitch Backstepping	3.97	0	6.04
Yaw PID	3.81	0	7.12
Yaw Lyapunov-based	3.25	0	-
Yaw Backstepping	3.97	0	0
Altitude PID	3.72	0.9	9.28
Altitude Lyapunov-based	3.07	3.8	-
Altitude Backstepping	3.89	0	6.44

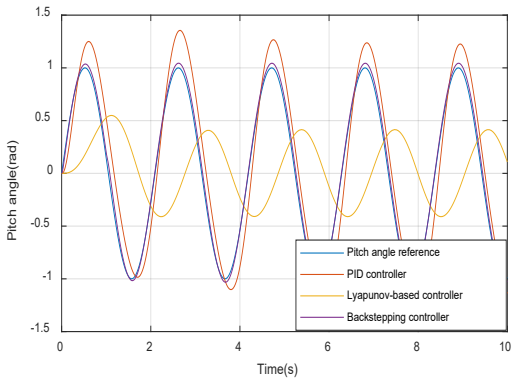

Figure 9. Pitch tracking for sinusoidal reference

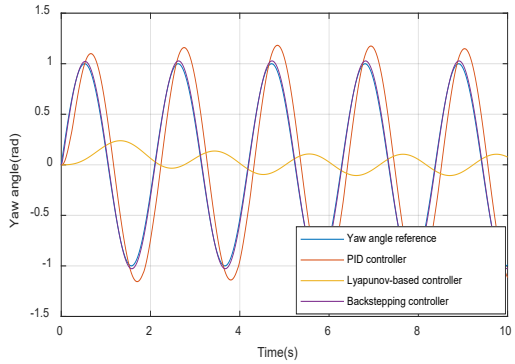

Figure 10. Yaw tracking for sinusoidal reference

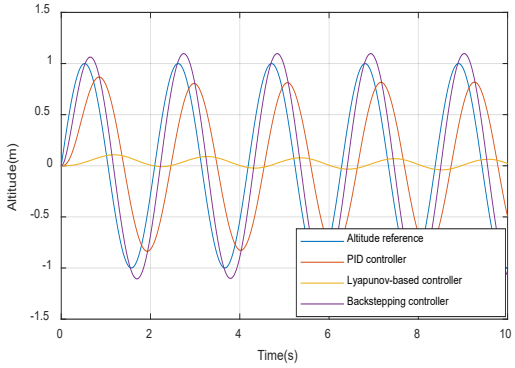

Figure 11. Altitude tracking for sinusoidal reference

Table 6 shows the time response data of the controllers for tracking a 3 rad/s sinusoidal wave.

The PID controller has the fastest rise time in all references. However, the PID controller also shows the highest overshoot. Additionally, it does not have a settling time, as it cannot settle within the ± 5% of the reference. Since the Lyapunov-based controller cannot rise to 90% of the reference value, there is no rise time. Since it does not reach the maximum point of the given reference values, it does not show any overshoot. Moreover, since it cannot follow the reference stably, it has no settling time. The backstepping control design has a rise time very close to PID controller, except for the altitude reference. It is the control design that shows the least overshoot and it is also the only controller that has a settling time in all references. It has the fastest settling time. Therefore, it is the most robust control design.

4.3 Sawtooth Wave Simulations

In this subsection, reference tracking was performed under a sawtooth wave with amplitude 3 and frequency 1 rad/s. Sawtooth wave tracking simulations are shown in Figures (12) to (15).

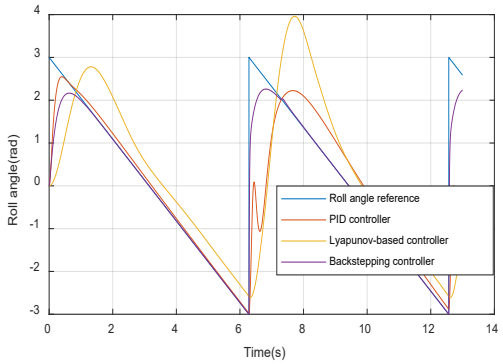

Figure 12. Roll tracking for sawtooth reference

Table 6. Time response for sinusoidal reference

Controller	Rise time (s)	Overshoot (%)	Settling time (s)
Roll PID	0.32	23.7	-
Roll Lyapunov-based	-	0	-
Roll Backstepping	0.31	3.2	0
Pitch PID	0.31	37.1	-
Pitch Lyapunov-based	-	0	-
Pitch Backstepping	0.29	4.6	0.69
Yaw PID	0.27	19.2	-
Yaw Lyapunov-based	-	0	-
Yaw Backstepping	0.30	2.72	0
Altitude PID	0.55	0	-
Altitude Lyapunov-based	-	0	-
Altitude Backstepping	0.37	9.62	2.48

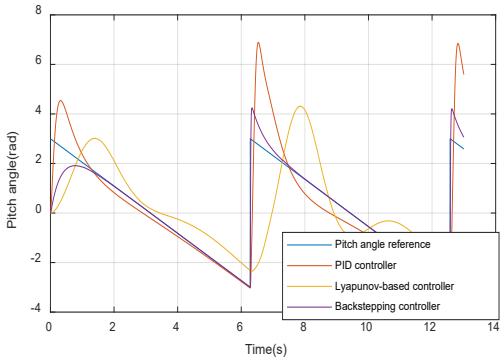

Figure 13. Pitch tracking for sawtooth reference

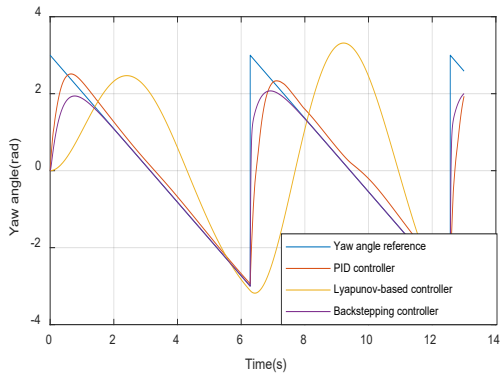

Figure 14. Yaw tracking for sawtooth reference

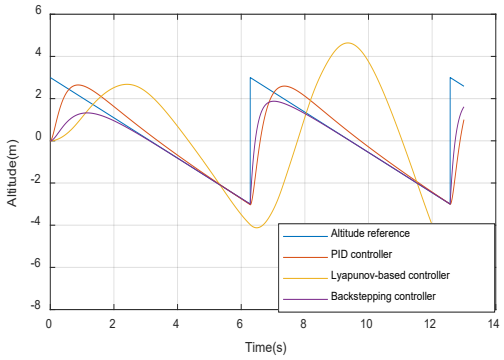

Figure 15. Altitude tracking for sawtooth reference

Table 7 shows the time response data of the controllers for tracking a sawtooth wave.

When the data in Table 7 is analyzed, it is observed that PID controller has the fastest rise time. However, since it cannot be within the ± 5% of the reference value, there is no settling time data and it shows a high overshoot. There is no settling time data for the Lyapunov-based controller, because it cannot be placed within the 5% range of the references. It shows the highest overshoot in all reference tracking, except the pitch angle reference. The backstepping controller is the only controller that shows no overshoot, except for the pitch reference. It is also the only controller that has settling time in all references. Therefore, it turns out that the backstepping controller is more successful in sawtooth wave reference tracking.

5. Conclusion

In this research, nonlinear modelling of a quadcopter was carried out. Then, a backstepping controller design that could perform aggressive maneuvers was developed. Simulations have been made for triangular, sinusoidal and sawtooth wave references. Within the scope of the study, the proposed backstepping controller was compared with PID and Lyapunov-based control structures. Robustness analysis was realized by comparing the time response of the controllers. As a result of this analysis, it was observed that the backstepping controller showed the least overshoot in all simulations and was the only controller with a settling time in all reference tracking. Thus, the superiority of the backstepping controller has been proven.

Table 7. Time response for sawtooth reference

Controller	Rise time (s)	Overshoot (%)	Settling time (s)
Roll PID	-	11.7	-
Roll Lyapunov-based	0.88	33.3	-
Roll Backstepping	-	0	0.89
Pitch PID	0.067	131.2	-
Pitch Lyapunov-based	0.834	45.4	-
Pitch Backstepping	6.22	41.6	13.5
Yaw PID	-	0	-
Yaw Lyapunov-based	8.7	12.2	-
Yaw Backstepping	-	0	13.5
Altitude PID	0.723	0	-
Altitude Lyapunov-based	1.836	56.8	-
Altitude Backstepping	-	0	13.39

REFERENCES

AbdulSamed, B. N., Aldair, A. A. & Al-Mayyahi, A. (2020) Robust trajectory tracking control and obstacles avoidance algorithm for quadrotor unmanned aerial vehicle. *Journal of Electrical Engineering & Technology*. 15(2), 855-868. doi: 10.1007/s42835-020-00350-8.

Dobrea, M. A., Iliescu, S. S., Arghira, N. & Vasluianu, M. (2023) Modeling of a Hybrid Controller for Electric Vehicle Battery Charging Using Photovoltaic Panels. *Studies in Informatics and Control*. 32(4), 27-35. doi:10.24846/v32i4y202303.

Elhesasy, M., Dief, T. N., Atallah, M., Okasha, M., Kamra, M. M., Yoshida, S. & Rushdi, M. A. (2023) Non-linear model predictive control using CasADi package for trajectory tracking of quadrotor. *Energies*. 16(5), 2143. doi: 10.3390/en16052143.

Frigioescu, T. F., Condruz, M. R., Badea, T. A. & Paraschiv, A. (2023) A Preliminary Study on the Development of a New UAV Concept and the Associated Flight Method. *Drones*. 7(3), 166. doi: 10.3390/drones7030166.

Karahan, M., Kasnakoglu, C. & Akay, A. N. (2023) Robust Backstepping Control of a Quadrotor UAV Under Pink Noise and Sinusoidal Disturbance. *Studies in Informatics and Control*. 32(2) 15-24. doi: 10.24846/v32i2y202302.

Karahan, M. & Kasnakoglu, C. (2021) Modeling a Quadrotor Unmanned Aerial Vehicle and robustness analysis of different controller designs under parameter uncertainty and noise disturbance. *Journal of Control Engineering and Applied Informatics*. 23(4), 13-24.

Kidambi, K. B., Fermüller, C., Aloimonos, Y. & Xu, H. (2021) Robust nonlinear control-based trajectory tracking for quadrotors under uncertainty. *IEEE Control Systems Letters*. 5(6), 2042-2047. doi: 10.1109/LCSYS.2020.3044833.

Krishna, A. B. & Kothari, M. (2022) Robust Geometric Trajectory Tracking Control of a Variable-Pitch Quadrotor. *Journal of Guidance, Control, and Dynamics*. 45(5), 902-920. doi: 10.2514/1.G006310.

Lavaei, R. & Bridgeman, L. J. (2023) Systematic, lyapunov-based, safe and stabilizing controller synthesis for constrained nonlinear systems. *IEEE Transactions on Automatic Control*. 69(5), 3011-3023. doi: 10.1109/TAC.2023.3302789.

Liu, K., Yang, P., Wang, R., Jiao, L., Li, T. & Zhang, J. (2023) Observer-based adaptive fuzzy finite-time attitude control for quadrotor UAVs. *IEEE Transactions on Aerospace and Electronic Systems*. 59(6), 8637-8654. doi: 10.1109/TAES.2023.3308552.

Mehmood, Y., Aslam, J., Ullah, N., Chowdhury, M. S., Techato, K. & Alzaed, A. N. (2021) Adaptive robust trajectory tracking control of multiple quad-rotor UAVs with parametric uncertainties and disturbances. *Sensors*. 21(7), 2401. doi: 10.3390/s21072401.

Nekoo, S. R., Acosta, J. Á. & Ollero, A. (2022) Quaternion-based state-dependent differential Riccati equation for quadrotor drones: Regulation control problem in aerobatic flight. *Robotica*. 40(9), 3120-3135. doi: 10.1017/S0263574722000091.

Pan, J., Shao, B., Xiong, J. & Zhang, Q. (2023) Attitude control of quadrotor UAVs based on adaptive sliding mode. *International Journal of Control, Automation and Systems*. 21(8), 2698-2707. doi: 10.1007/s12555-022-0189-2.

Saeed, A. S., Younes, A. B., Cai, C. & Cai, G. (2018) A survey of hybrid unmanned aerial vehicles. *Progress in Aerospace Sciences*. 98, 91-105. doi: 10.1016/j.paerosci.2018.03.007.

Sonugur, G. (2023) A Review of quadrotor UAV: Control and SLAM methodologies ranging from conventional to innovative approaches. *Robotics and Autonomous Systems*. 161, 104342. doi: 10.1016/j.robot.2022.104342.

Sun, W., Zhang, X., Lin, G., Wang, H. & Han, J. (2021) Extreme Maneuvering Control and Planning of Multi-Rotor UAV for High-Speed Invading Target Avoidance. In: *2021 IEEE International Conference on Real-time Computing and Robotics (RCAR)*, *15-19 July 2021, Xining, China*. New Jersey, U.S.A., Institute of Electrical and Electronics Engineers (IEEE). pp. 387-392. doi: 10.1109/RCAR52367.2021.9517525.

Wang, B., Zhang, Y. & Zhang, W. (2022) Integrated path planning and trajectory tracking control for quadrotor UAVs with obstacle avoidance in the presence of environmental and systematic uncertainties: Theory and experiment. *Aerospace Science and Technology*. 120, 107277. doi: 10.1016/j.ast.2021.107277.

Zhang, Z., Wang, Q., Ge, S. S. & Zhang, Y. (2021) Reduced-order filters-based adaptive backstepping control for perturbed nonlinear systems. *IEEE Transactions on Cybernetics*. 52(8), 8388-8398. doi: 10.1109/TCYB.2021.3049786.

Zhao, Z., Cao, D., Yang, J. & Wang, H. (2020) High-order sliding mode observer-based trajectory tracking control for a quadrotor UAV with uncertain dynamics. *Nonlinear Dynamics*. 102, 2583-2596. doi: 10.1007/s11071-020-06050-2.

Zhou, S., Lin, W., Mao, X. & Wu, J. (2023) Generalized invariance principles for stochastic dynamical systems and their applications. *IEEE Transactions on Automatic Control*. 69(1), 85-99. doi: 10.1109/TAC.2023.3274215.